PROCEEDINGS OF SCIENCE

Global fits of $b \to d\,\ell^+\ell^-$

Hector Gisbert[a,*]

[a] *Dipartimento di Fisica e Astronomia 'G. Galilei', Università di Padova, Via F. Marzolo 8, 35131 Padova, Italy*

E-mail: hector.gisbert@pd.infn.it

We conduct a model-independent analysis of processes involving $|\Delta b| = |\Delta d| = 1$ transitions, aiming to test the standard model and explore flavor patterns of new physics. Exploiting the current data from $B^+ \to \pi^+\mu^+\mu^-$, $B_s^0 \to \bar{K}^{*0}\mu^+\mu^-$, $B^0 \to \mu^+\mu^-$, and radiative $B \to X_d\,\gamma$ decays, we derive constraints on Wilson coefficients through global fits. The fit results are consistent with the standard model but show significant potential for new physics contributions at experimental facilities like LHCb and Belle II, or a future e^+e^- collider.

21st Conference on Flavor Physics and CP Violation (FPCP 2023)
29 May - 2 June 2023
Lyon, France

*Speaker

PoS(FPCP2023)057

1. Introduction

Flavor-changing neutral current (FCNC) transitions provide an excellent avenue for probing new physics (NP). In the Standard Model (SM), these transitions occur via loops and are suppressed by the Cabibbo-Kobayashi-Maskawa (CKM) mechanism. These suppressions make them exceptionally sensitive to contributions beyond the SM (BSM), which could potentially have comparable effects to the SM ones. Furthermore, adding leptons to the FCNC transitions leads to rare decays where the universality of lepton couplings within the SM makes them ideal for testing lepton universality (LU) and lepton flavor conservation (LFC). These characteristics collectively position rare decays as an exceptional window for exploring BSM physics.

Rare radiative decays $b \to q\,\gamma$ and semileptonic decays $b \to q\,\ell^-\ell^+$, where $q = s, d$, and $\ell = e, \mu, \tau$, stand as effective tools for scrutinizing these fundamental SM symmetries in the down sector. Among them, transitions like $b \to s\,\mu^+\mu^-$ have exhibited deviations from SM predictions in terms of branching ratios and angular distributions in the last decade [1–3]. However, the recent experimental update on the R_K ratio by LHCb [4, 5], which consistently aligns with the SM predictions, introduces further complexity in the BSM sources behind the observed tensions from the SM in global fits [6–10].

Given the current hints of NP in $b \to s\,\mu^+\mu^-$ transitions, it is imperative to perform further cross-checks in other sectors like $b \to d\,\mu^+\mu^-$. The main objective of this work [11] is to provide a comprehensive analysis of $|\Delta b| = |\Delta d| = 1$ processes using available data. Through model-independent global fits, we derive stringent constraints on the Wilson coefficients and investigate their interplay with $b \to s\,\mu^+\mu^-$ transitions. The results presented in this work could offer further insights into these tensions as new data becomes available. For earlier analyses see Refs. [12–14].

The paper is organized as follows: Section 2 introduces the effective theory framework employed to analyze $b \to q\,\mu^+\mu^-$ transitions. Section 3 outlines the rare decay observables included in our analysis. In Section 4, we present the results of our 1D and 2D global fit for $b \to d\,\mu^+\mu^-$ transitions and the comparison with $b \to s\,\mu^+\mu^-$ global fits. Section 5 concludes with our main findings. Further details can be found in Ref. [11].

2. Effective theory approach to rare B decays

The weak effective theory framework for studying $|\Delta b| = |\Delta q| = 1$ transitions is given by the following effective Hamiltonian

$$\mathcal{H}_{\text{eff}} \supset -\frac{4\,G_{\text{F}}}{\sqrt{2}}\,V_{tq}^*V_{tb}\,\sum_{i=7}^{10}\left(c_i\,O_i + c_i'\,O_i'\right) + \text{h.c.}\,. \tag{1}$$

The Wilson coefficients $c_i = C_i^{\text{SM}} + C_i$ and $c_i' = C_i'$ account for both SM and NP effects from the following dimension-six operators

$$O_7^{(\prime)} = \frac{e}{16\pi^2}m_b\left(\bar{q}_{L(R)}\sigma^{\alpha\beta}b_{R(L)}\right)F_{\alpha\beta}\,, \tag{2}$$

$$O_8^{(\prime)} = \frac{g_s}{16\pi^2}m_b\left(\bar{q}_{L(R)}\sigma^{\alpha\beta}T^a b_{R(L)}\right)G^a_{\alpha\beta}\,, \tag{3}$$

$$O_9^{(\prime)} = \frac{\alpha_e}{4\pi}\left(\bar{q}_{L(R)}\gamma_\alpha b_{L(R)}\right)\left(\bar{\mu}\gamma^\alpha\mu\right)\,, \tag{4}$$

$$O_{10}^{(\prime)} = \frac{\alpha_e}{4\pi}\left(\bar{q}_{L(R)}\gamma_\alpha b_{L(R)}\right)\left(\bar{\mu}\gamma^\alpha\gamma^5\mu\right)\,. \tag{5}$$

At $\mu_b \approx m_b$, the SM predictions on the Wilson coefficients are $C_7^{\rm SM}(\mu_b) = -0.30$, $C_8^{\rm SM}(\mu_b) = -0.15$, $C_9^{\rm SM}(\mu_b) = 4.12$, and $C_{10}^{\rm SM}(\mu_b) = -4.18$ [13]. The contributions to the primed Wilson coefficients suffer from a strong suppression due to the light quark mass and therefore can be safely neglected in the SM, along with (pseudo-)scalar and (pseudo-)tensor operators.

3. $|\Delta b| = |\Delta d| = 1$ observables

In this section, we provide the $|\Delta b| = |\Delta d| = 1$ observables included in the global fits presented in Section 4. For details, we refer to Ref. [11], where the expressions for these observables are either directly provided or appropriately adapted from Refs. [13, 15, 16].

3.1 $B^+ \to \pi^+\mu^+\mu^-$

In this subsection, we present binned branching fractions for $B^+ \to \pi^+\mu^+\mu^-$. LHCb measurements [17] (fourth column in 1) agree well with SM predictions (third column in 1). All bins are within $1\,\sigma$, except the high-q^2 bin [22, 25] GeV^2, which agrees at $1.6\,\sigma$. Regions around $q^2 \approx 9.5\,\text{GeV}^2$ and $q^2 \approx 13.5\,\text{GeV}^2$ suffer from J/ψ and ψ' resonances. For global fits (discussed in Section 4), only bins $k = 1, 2, 9$ are included, corresponding to intervals [2, 4] GeV^2, [4, 6] GeV^2, and [15, 22] GeV^2, respectively.

k	$[q^2_{\rm min}, q^2_{\rm max}]$	$\mathcal{B}_k^{(B\pi)}$	
		SM	experiment
	[GeV^2]	[10^{-9} GeV^{-2}]	[10^{-9} GeV^{-2}]
1	[2, 4]	$0.80 \pm 0.12 \pm 0.05 \pm 0.04$	$0.62^{+0.39}_{-0.33} \pm 0.02$
2	[4, 6]	$0.81 \pm 0.12 \pm 0.05 \pm 0.05$	$0.85^{+0.32}_{-0.27} \pm 0.02$
3	[6, 8]	$0.82 \pm 0.11 \pm 0.05 \pm 0.07$	$0.66^{+0.30}_{-0.25} \pm 0.02$
4	[11, 12.5]	$0.82 \pm 0.09 \pm 0.05 \pm 0.09$	$0.88^{+0.34}_{-0.29} \pm 0.03$
5	[15, 17]	$0.73 \pm 0.06 \pm 0.04 \pm 0.06$	$0.63^{+0.24}_{-0.19} \pm 0.02$
6	[17, 19]	$0.67 \pm 0.05 \pm 0.04 \pm 0.05$	$0.41^{+0.21}_{-0.17} \pm 0.01$
7	[19, 22]	$0.57 \pm 0.03 \pm 0.03 \pm 0.04$	$0.38^{+0.18}_{-0.15} \pm 0.01$
8	[22, 25]	$0.35 \pm 0.02 \pm 0.02 \pm 0.02$	$0.14^{+0.13}_{-0.09} \pm 0.01$
9	[15, 22]	$0.64 \pm 0.04 \pm 0.04 \pm 0.05$	$0.47^{+0.12}_{-0.10} \pm 0.01$
10	$[4m_\mu^2, (m_{B^+} - m_{\pi^+})^2]$	$17.9 \pm 1.9 \pm 1.1 \pm 1.5^\dagger$ GeV^2	$18.3 \pm 2.4 \pm 0.5$ GeV^2

Figure 1: SM non-resonant binned branching fractions $\mathcal{B}_k^{(B\pi)}$ are provided in units of $10^{-9}\,\text{GeV}^2$. SM predictions appear in the third column with associated uncertainties stemming from form factors (FFs), CKM matrix elements, and μ_b, respectively. Experimental central values from LHCb [17] are in the last column, together with the statistical and systematic uncertainties.

In the presence of NP, these observables can be parametrized as $\mathcal{B}_k^{(B\pi)} = \sum_i a_i^{(B\pi)}\, w^{(B\pi)}$ being sensitive to the following set of Wilson coefficient combinations

$$w^{(B\pi)} = \left\{1,\, C_{7^+},\, C_{8^+},\, C_{9^+},\, C_{10^+},\, C_{7^+}^2,\, C_{8^+}^2,\, C_{9^+}^2,\, C_{10^+}^2,\, C_{7^+}\cdot C_{8^+},\, C_{7^+}\cdot C_{9^+},\, C_{8^+}\cdot C_{9^+}\right\}\,, \tag{6}$$

where $C_{i^\pm} = C_i \pm C_i'$. The values of $a_i^{(B\pi)}$ for different bins k are given in Table II from Ref. [11].

3.2 $B_s^0 \to \bar{K}^{*0}\mu^+\mu^-$

The SM prediction of the integrated differential branching ratio of $B_s^0 \to \bar{K}^{*0}\mu^+\mu^-$ decay reads [11]

$$\mathcal{B}(B_s^0 \to \bar{K}^{*0}\mu^+\mu^-)_{\rm SM}^{[0.1,19]\,\rm GeV^2} = (46.0 \pm 2.1 \pm 2.8 \pm 3.3 \pm 3.6) \cdot 10^{-9}\,, \tag{7}$$

in agreement with the experimental measurement from LHCb, $\mathcal{B}(B_s^0 \to \bar{K}^{*0}\mu^+\mu^-)_{\rm exp} = (29 \pm 11) \cdot 10^{-9}$ [18]. Eq. (7) displays the four sources of uncertainty: FFs, CKM elements, μ_b renormalization scale, and the impact of J/ψ and ψ' resonances.

Thanks to Lorentz invariance and parity conservation of QCD, the NP effects enter either as a sum C_{i^+} or a difference C_{i^-} with the unprimed coefficients, resulting in $\mathcal{B}(B_s^0 \to \bar{K}^{*0}\mu^+\mu^-) = \sum_i a_i^{(B_s\bar{K}^*)}\, w_i^{(B_s\bar{K}^*)}$, and the following set of Wilson coefficients

$$\begin{aligned} w_i^{(B_s\bar{K}^*)} = \big\{&1,\, C_7,\, C_8,\, C_9,\, C_{10},\, C_7^2,\, C_8^2,\, C_9^2,\, C_{10}^2,\, C_7',\, C_8',\, C_9',\, C_{10}',\, (C_7')^2,\, (C_8')^2,\, (C_9')^2,\\ &(C_{10}')^2,\, C_7\cdot C_7',\, C_8\cdot C_8',\, C_9\cdot C_9',\, C_{10}\cdot C_{10}',\, C_7\cdot C_8,\, C_7'\cdot C_8,\, C_7\cdot C_8',\, C_7'\cdot C_8'\\ &C_7\cdot C_9,\, C_7'\cdot C_9,\, C_7\cdot C_9',\, C_7'\cdot C_9'\, C_8\cdot C_9,\, C_8'\cdot C_9,\, C_8\cdot C_9',\, C_8'\cdot C_9'\big\}\,. \end{aligned} \tag{8}$$

The values of $a_i^{(B_s\bar{K}^*)}$ for the q^2-region $[0.1,\ 19]\ \rm GeV^2$ are given in Table III from Ref. [11].

3.3 $B^0 \to \mu^+\mu^-$

$B^0 \to \mu^+\mu^-$ is a clean probe for BSM physics in $b \to d\,\mu^+\mu^-$ transitions. In the SM, only the operator O_{10} contributes, which yields [11]

$$\mathcal{B}(B^0 \to \mu^+\mu^-)_{\rm SM} \;=\; (1.01 \pm 0.07) \cdot 10^{-10}\,, \tag{9}$$

in agreement with the experimental value $\mathcal{B}(B^0 \to \mu^+\mu^-)_{\rm exp} = (1.20 \pm 0.84) \cdot 10^{-10}$ [19]. Including NP effects from C_{10}, the branching ratio can be written as

$$\frac{\mathcal{B}(B^0 \to \mu^+\mu^-)}{\mathcal{B}(B^0 \to \mu^+\mu^-)_{\rm SM}} = \left|\frac{C_{10}^{\rm SM} + C_{10^-}}{C_{10}^{\rm SM}}\right|^2\,, \tag{10}$$

which leads to the following ranges for C_{10^-}:

$$-1.8 \lesssim C_{10^-} \lesssim 1.7 \quad \text{or} \quad 6.7 \lesssim C_{10^-} \lesssim 10.1\,, \tag{11}$$

when combined with the experimental information. The first range corresponds to NP corrections close to the SM, while the second one involves large cancellations with the SM, $C_{10^-} \approx -2\,C_{10}^{\rm SM}$. Future $300\,\rm fb^{-1}$ LHC projections will allow an uncertainty reduction of ~ 6 [20], implying the following constraints on C_{10^-},

$$-0.3 \lesssim C_{10^-} \lesssim 0.3 \text{ or } 8.1 \lesssim C_{10^-} \lesssim 8.6\,(\text{HL-LHC})\,, \tag{12}$$

if SM central values are assumed.

3.4 $b \to d\,\gamma$

The SM prediction for the CP-averaged $\bar{B} \to X_d\,\gamma$ branching ratio reads $\mathcal{B}(\bar{B} \to X_d\,\gamma)_{\rm SM} = (16.8 \pm 1.7) \cdot 10^{-6}$ [11], in very good agreement with the extrapolated experimental value from BaBar [21, 22], $\mathcal{B}(\bar{B} \to X_d\,\gamma)_{\rm exp} = (14.1 \pm 5.7) \cdot 10^{-6}$. Including NP effects from $C_{7,8}^{(\prime)}$ using Ref. [16], we find the following parametrization $\mathcal{B}(\bar{B} \to X_d\,\gamma) = \sum_i a_i^{(\bar{B}X_d)}\, w_i^{(\bar{B}X_d)}$, with the following combinations of Wilson coefficients

$$w_i^{(\bar{B}X_d)} = \left\{1,\, C_7,\, C_8,\, C_7^2,\, C_8^2,\, (C_7')^2,\, (C_8')^2,\, C_7 \cdot C_8,\, C_7' \cdot C_8'\right\} . \tag{13}$$

The central values of the factors $a_i^{(\bar{B}X_d)}$ are compiled in Table IV from Ref. [11].

4. Global fits

In the following, we present the $|\Delta b| = |\Delta d| = 1$ fit outcomes for 1D and 2D analyses involving different NP Wilson coefficients: $C_7^{(\prime)}$, $C_8^{(\prime)}$, $C_9^{(\prime)}$, and $C_{10}^{(\prime)}$. The fit approach is detailed in Ref. [11].

4.1 1D fits

Table 2 displays results from the 1D scenarios ($H_{1,\ldots,16}$). The first column denotes the scenario name, and the second column indicates the fitted Wilson coefficient. Best-fit values with 1σ and 2σ confidence intervals are presented in the third and fourth columns. The final columns indicate goodness-of-fit indicators. While we observe an excellent agreement with the SM, it is interesting to note that among the NP scenarios, those involving C_9 exhibit the largest (albeit still insignificant) pull, which aligns with observations in $b \to s$ transitions. Similar remarks are applicable in subsection 4.2.

Although we observe an excellent agreement with the SM, among the NP scenarios it is interesting to note that the ones with C9 are giving the largest (still insignificant) pull, which fits observations in b->s. Similar comments apply in subsection 4.2.

For scenarios involving only one Wilson coefficient at a time, $H_{1,\ldots,8}$, the favored option is H_3 with NP in C_9 only (pull of $1.63\,\sigma$ and $p-$value of 95%). This scenario is followed by H_4 with NP in C_{10} (pull of $1.50\,\sigma$ and $p-$value of 91%).

In scenarios with two Wilson coefficients, H_{10} with left-handed quarks and left-handed leptons, $C_9 = -\,C_{10}$, stands out (pull of $1.58\,\sigma$ and $p-$value of 93%). In contrast the benchmark H_9 with left-handed quarks and right-handed leptons $C_9 = C_{10}$ has a pull of $0.24\,\sigma$ and $p-$value of 59%, worse than the SM one. We observe similar findings to the ones in $b \to s$ transitions where a good fit is obtained for $C_9^{(b\to s)} = -\,C_{10}^{(b\to s)} = -\,0.50 \pm 0.13$, see Ref. [11].

In conclusion, data highlights a preference for NP via C_9, mirroring the trend seen in global fits to $b \to s\,\mu^+\mu^-$ data.

4.2 2D fits

Table VI in Ref. [11] presents the 2D fit results. Similar to the 1D fit results, we note that including C_9 in the 2D fits leads to large $p-$values, around 90%. Figure 3 show as example the 2D fit contour for the Wilson coefficients C_9 and C_{10} (scenario H_{23}). Collaborative contributions

scenario	fit parameter	best fit	1σ	2σ	$\chi^2_{H_i,\,\mathrm{min}}$	Pull_{H_i}	p-value (%)
H_1	C_7	0.01	[-0.07, 0.11]	[-0.15, 0.25]	3.74	0.15	58
H_2	C_8	0.04	[-0.88, 1.44]	[-1.51, 2.27]	3.76	0.04	58
H_3	C_9	-1.37	[-2.97, -0.47]	[-7.65, 0.26]	1.12	1.63	95
H_4	C_{10}	0.96	[0.3, 1.75]	[-0.29, 2.92]	1.51	1.50	91
H_5	C_7'	-0.02	[-0.18, 0.16]	[-0.31, 0.3]	3.75	0.11	58
H_6	C_8'	-0.04	[-1.16, 1.13]	[-1.86, 1.85]	3.76	0.03	58
H_7	C_9'	-0.21	[-0.91, 0.47]	[-1.63, 1.15]	3.67	0.32	59
H_8	C_{10}'	0.22	[-0.37, 0.8]	[-0.98, 1.38]	3.63	0.37	60
H_9	$C_9 = +C_{10}$	0.19	[-0.57, 1.02]	[-1.24, 1.79]	3.71	0.24	59
H_{10}	$C_9 = -C_{10}$	-0.53	[-0.89, -0.19]	[-1.29, 0.14]	1.27	1.58	93
H_{11}	$C_9' = +C_{10}'$	0.10	[-0.68, 0.86]	[-1.41, 1.53]	3.75	0.13	58
H_{12}	$C_9' = -C_{10}'$	-0.13	[-0.46, 0.22]	[-0.8, 0.57]	3.63	0.37	60
H_{13}	$C_9 = -C_9'$	-1.74	[-3.26, -0.27]	[-4.04, 0.44]	1.96	1.34	85
H_{14}	$C_9 = +C_9'$	-0.55	[-1.29, -0.07]	[-4.13, 0.34]	2.42	1.16	78
H_{15}	$C_9 = -C_{10} = -C_9' = -C_{10}'$	-0.58	[-1.06, -0.2]	[-4.04, 0.12]	1.17	1.61	94
H_{16}	$C_9 = -C_{10} = +C_9' = -C_{10}'$	-0.24	[-0.46, -0.04]	[-0.7, 0.16]	2.35	1.19	79

Figure 2: Fit results for Wilson coefficients in the 1D scenarios ($H_{1,\ldots,16}$) are presented at scale μ_b. Best-fit values and 1σ (2σ) uncertainties are shown in the third and fourth (fifth) columns. Goodness-of-fit indicators are in the final columns: χ^2 at best-fit, Pull_{H_i} in standard deviation units, and $p-$value. The SM yields $\chi^2_{\mathrm{SM}} = 3.77$, with a 71% $p-$value.

from $B^+ \to \pi^+\mu^+\mu^-$ and $B_s^0 \to \bar{K}^{0*}\mu^+\mu^-$ reduce the annulus thickness (red area), but the C_9 and C_{10} degeneracy persists. While $B^0 \to \mu^+\mu^-$ has the potential to resolve this, current precision falls short. In the future, the HL-LHC run could greatly improve the situation, Eq. (12), illustrated by dashed blue lines in Figure 3.

Assuming minimal quark flavor violation, $b \to s$ fits can be linked to $b \to d$ ones. In the weak effective theory (1), this implies universal C_i coefficients, allowing direct comparison between both fits. The discrepancy between $b \to s$ and $b \to d$ Wilson coefficients would imply extra sources of quark flavor violation beyond the SM. Figure 3 includes the $b \to d$ (red) and $b \to s$ (blue) global fit results for the same scenario. The exclusion of the SM (black star) from the $b \to s$ preferred regions reflects the current B anomalies. The $b \to s$ preferred region lies within the $b \to d$ one. Thus, data is consistent with the minimal quark flavor violation hypothesis. Further validation requires improved data on $b \to d$ transitions.

5. Conclusions

In summary, this study presents a model-independent analysis of rare radiative and semileptonic processes involving $|\Delta b| = |\Delta d| = 1$. The data demonstrate consistency with SM predictions, while

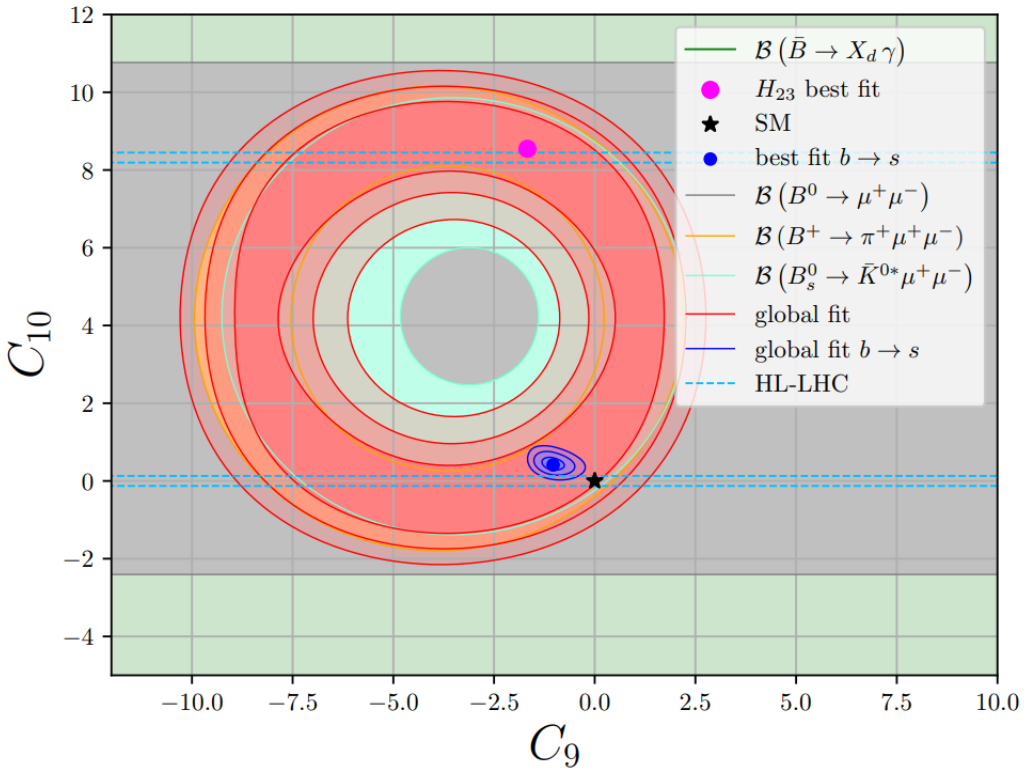

Figure 3: 2D fit contour of the Wilson coefficients C_9, C_{10} (scenario H_{23}). We show the 1σ allowed regions of the individual observables and the combined 1, 2, and 3 σ regions (red). The black star at the origin symbolizes the SM. Overlaid in blue are the results of the global $b \to s$ fit from Ref. [11], serving as a data-driven prediction assuming minimal flavor violation (MFV).

also allowing substantial room for NP. The branching ratios of $b \to d\,\mu^+\mu^-$ transitions exhibit a suppression pattern similar to that seen in $b \to s\,\mu^+\mu^-$, albeit with wider ranges of uncertainty. Improving fit results depends not only on increasing statistics but also on incorporating observables sensitive to various Wilson coefficient combinations, such as angular observables. While these fits align with the SM, they strongly suggest the potential for constraining NP contributions, especially at experimental facilities like LHCb, Belle II, or a future e^+e^- collider.

Acknowledgements

I would like to thank the organizers of FPCP 2023 for the invitation, and for their efforts in making this conference a great success. Thanks also to Rigo Bause, Marcel Golz, and Gudrun Hiller for enjoyable collaborations.

References

[1] S. Bifani, S. Descotes-Genon, A. Romero Vidal and M. H. Schune, J. Phys. G **46** (2019) no.2, 023001 [arXiv:1809.06229 [hep-ex]].

[2] J. Albrecht, D. van Dyk and C. Langenbruch, Prog. Part. Nucl. Phys. **120** (2021), 103885 [arXiv:2107.04822 [hep-ex]].

[3] D. London and J. Matias, Ann. Rev. Nucl. Part. Sci. **72** (2022), 37-68 [arXiv:2110.13270 [hep-ph]].

[4] R. Aaij *et al.* [LHCb], Phys. Rev. D **108** (2023) no.3, 032002 [arXiv:2212.09153 [hep-ex]].

[5] R. Aaij *et al.* [LHCb], Phys. Rev. Lett. **131** (2023) no.5, 051803 [arXiv:2212.09152 [hep-ex]].

[6] M. Algueró, B. Capdevila, S. Descotes-Genon, J. Matias and M. Novoa-Brunet, Eur. Phys. J. C **82** (2022) no.4, 326 [arXiv:2104.08921 [hep-ph]].

[7] J. Kriewald, C. Hati, J. Orloff and A. M. Teixeira, [arXiv:2104.00015 [hep-ph]].

[8] L. S. Geng, B. Grinstein, S. Jäger, S. Y. Li, J. Martin Camalich and R. X. Shi, Phys. Rev. D **104** (2021) no.3, 035029 [arXiv:2103.12738 [hep-ph]].

[9] R. Bause, H. Gisbert, M. Golz and G. Hiller, JHEP **12** (2021), 061 [arXiv:2109.01675 [hep-ph]].

[10] F. Mahmoudi, [arXiv:2208.05755 [hep-ph]].

[11] R. Bause, H. Gisbert, M. Golz and G. Hiller, Eur. Phys. J. C **83** (2023) no.5, 419 [arXiv:2209.04457 [hep-ph]].

[12] D. Du, A. X. El-Khadra, S. Gottlieb, A. S. Kronfeld, J. Laiho, E. Lunghi, R. S. Van de Water and R. Zhou, Phys. Rev. D **93** (2016) no.3, 034005 [arXiv:1510.02349 [hep-ph]].

[13] A. Ali, A. Y. Parkhomenko and A. V. Rusov, Phys. Rev. D **89** (2014) no.9, 094021 [arXiv:1312.2523 [hep-ph]].

[14] A. V. Rusov, JHEP **07** (2020), 158 [arXiv:1911.12819 [hep-ph]].

[15] A. Ali, P. Ball, L. T. Handoko and G. Hiller, Phys. Rev. D **61** (2000), 074024 [arXiv:hep-ph/9910221 [hep-ph]].

[16] T. Hurth, E. Lunghi and W. Porod, Nucl. Phys. B **704** (2005), 56-74 [arXiv:hep-ph/0312260 [hep-ph]].

[17] R. Aaij *et al.* [LHCb], JHEP **10** (2015), 034 [arXiv:1509.00414 [hep-ex]].

[18] R. Aaij *et al.* [LHCb], JHEP **07** (2018), 020 [arXiv:1804.07167 [hep-ex]].

[19] R. Aaij *et al.* [LHCb], Phys. Rev. D **105** (2022) no.1, 012010 [arXiv:2108.09283 [hep-ex]].

[20] A. Di Canto and S. Meinel, [arXiv:2208.05403 [hep-ex]].

[21] M. Misiak *et al.* Phys. Rev. Lett. **114** (2015) no.22, 221801 [arXiv:1503.01789 [hep-ph]].

[22] P. del Amo Sanchez *et al.* [BaBar], Phys. Rev. D **82** (2010), 051101 [arXiv:1005.4087 [hep-ex]].